NASA/TP-2004-212849

Debonding Stress Concentrations in a Pressurized Lobed Sandwich-Walled Generic Cryogenic Tank

William L. Ko
NASA Dryden Flight Research Center
Edwards, California

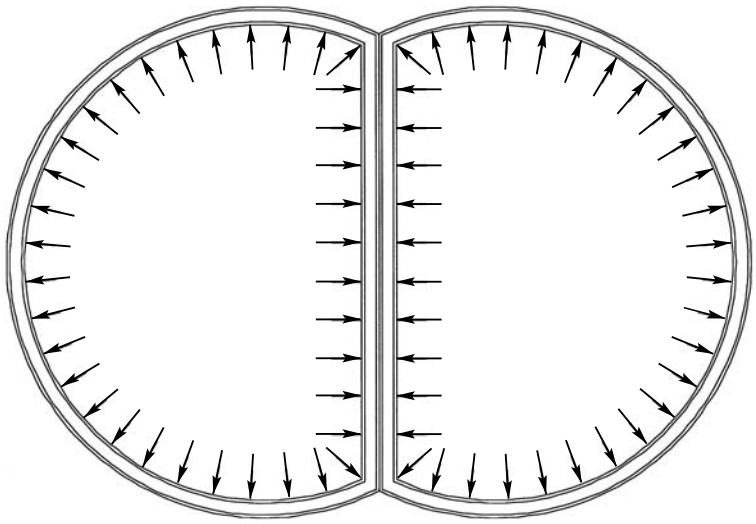

May 2004

The NASA STI Program Office…in Profile

Since its founding, NASA has been dedicated to the advancement of aeronautics and space science. The NASA Scientific and Technical Information (STI) Program Office plays a key part in helping NASA maintain this important role.

The NASA STI Program Office is operated by Langley Research Center, the lead center for NASA's scientific and technical information. The NASA STI Program Office provides access to the NASA STI Database, the largest collection of aeronautical and space science STI in the world. The Program Office is also NASA's institutional mechanism for disseminating the results of its research and development activities. These results are published by NASA in the NASA STI Report Series, which includes the following report types:

- TECHNICAL PUBLICATION. Reports of completed research or a major significant phase of research that present the results of NASA programs and include extensive data or theoretical analysis. Includes compilations of significant scientific and technical data and information deemed to be of continuing reference value. NASA's counterpart of peer-reviewed formal professional papers but has less stringent limitations on manuscript length and extent of graphic presentations.

- TECHNICAL MEMORANDUM. Scientific and technical findings that are preliminary or of specialized interest, e.g., quick release reports, working papers, and bibliographies that contain minimal annotation. Does not contain extensive analysis.

- CONTRACTOR REPORT. Scientific and technical findings by NASA-sponsored contractors and grantees.

- CONFERENCE PUBLICATION. Collected papers from scientific and technical conferences, symposia, seminars, or other meetings sponsored or cosponsored by NASA.

- SPECIAL PUBLICATION. Scientific, technical, or historical information from NASA programs, projects, and missions, often concerned with subjects having substantial public interest.

- TECHNICAL TRANSLATION. English-language translations of foreign scientific and technical material pertinent to NASA's mission.

Specialized services that complement the STI Program Office's diverse offerings include creating custom thesauri, building customized databases, organizing and publishing research results…even providing videos.

For more information about the NASA STI Program Office, see the following:

- Access the NASA STI Program Home Page at ***http://www.sti.nasa.gov***

- E-mail your question via the Internet to help@sti.nasa.gov

- Fax your question to the NASA Access Help Desk at (301) 621-0134

- Telephone the NASA Access Help Desk at (301) 621-0390

- Write to:
  NASA Access Help Desk
  NASA Center for AeroSpace Information
  7121 Standard Drive
  Hanover, MD 21076-1320

NASA/TP-2004-212849

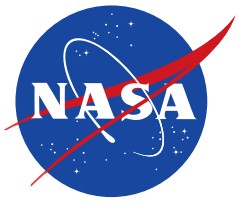

Debonding Stress Concentrations in a Pressurized Lobed Sandwich-Walled Generic Cryogenic Tank

William L. Ko
NASA Dryden Flight Research Center
Edwards, California

National Aeronautics and
Space Administration

Dryden Flight Research Center
Edwards, California 93523-0273

May 2004

Cover art: NASA Dryden Flight Research Center, art number 040095.

NOTICE

Use of trade names or names of manufacturers in this document does not constitute an official endorsement of such products or manufacturers, either expressed or implied, by the National Aeronautics and Space Administration.

Available from the following:

NASA Center for AeroSpace Information (CASI)
7121 Standard Drive
Hanover, MD 21076-1320
(301) 621-0390

National Technical Information Service (NTIS)
5285 Port Royal Road
Springfield, VA 22161-2171
(703) 487-4650

CONTENTS

ABSTRACT

A finite-element stress analysis has been conducted on a lobed composite sandwich tank subjected to internal pressure and cryogenic cooling. The lobed geometry consists of two obtuse circular walls joined together with a common flat wall. Under internal pressure and cryogenic cooling, this type of lobed tank wall will experience open-mode (a process in which the "honeycomb" is stretched in the depth direction) and shear stress concentrations at the junctures where curved wall changes into flat wall (known as a curve-flat juncture). Open-mode and shear stress concentrations occur in the honeycomb core at the curve-flat junctures and could cause debonding failure. The levels of contributions from internal pressure and temperature loading to the open-mode and shear debonding failure are compared. The lobed fuel tank with honeycomb sandwich walls has been found to be a structurally unsound geometry because of very low debonding failure strengths. The debonding failure problem could be eliminated if the honeycomb core at the curve-flat juncture is replaced with a solid core.

NOMENCLATURE

a	radius of tank wall, in.
A_c	cross-sectional area, normal to honeycomb cell generatrix, of unit honeycomb cell, in^2
A_w	cross-sectional area, normal to honeycomb cell generatrix, of unit honeycomb cell wall, in^2
d	size of right hexagonal honeycomb cell (maximum diagonal of honeycomb cell cross section), in.
E41	quadrilateral membrane elements
E31	triangular membrane elements
F_i	nodal force at inner surface node *i*, lb
h	depth of sandwich core, in.
i, j	indices, 1,2,3.....
JLOC	joint location
l	*x*-coordinate of center of circular region of tank wall, in.
p	internal pressure, lb/in^2
s_i	tangential coordinate of inner surface node *i*, in.
t_w	thickness of honeycomb cell wall, in.
t_1	thickness of inner face sheet, in.
t_2	thickness of outer face sheet, in.
T_1	inner face sheet temperature, °F
T_2	outer face sheet temperature, °F
x, y, z	rectangular Cartesian coordinates

δ_r tank wall radial displacement along *x*-axis, in.

δ_y curve-flat juncture displacement along *y*-direction, in.

θ angle subtended by the circular arc portion of tank wall, deg

ρ_c density of honeycomb core material, lb/in^3

ρ_{hc} effective density of honeycomb core structure, lb/in^3

σ_r effective radial stress, lb/in^2

σ_w actual radial stress induced in honeycomb cell wall, lb/in^2

σ_x stress in *x*-direction, lb/in^2

σ_y stress in *y*-direction, lb/in^2

σ_θ tangential stress, lb/in^2

$\tau_{r\theta}$ shear stress, lb/in^2

τ_{xy} shear stress in *x*-*y* plane, lb/in^2

INTRODUCTION

Bending a curved bar (monolithic, laminated composite, or sandwich bar) in the direction of reducing its curvature (that is, flattening the beam, known as open-mode bending) is known to induce radial tensile stress (open-mode stress) in the beam depth direction (refs. 1–7). For a solid curved beam, the induced open-mode stress distribution across the beam depth is arch shaped. The two zero stress points are located at the inner and outer boundaries, and the maximum stress point is located at the inward vicinity of the middle surface (refs. 1–5). The magnitude of the open-mode stress is proportional to the bending moment and inversely proportional to the product of core depth and the radius of the curved beam (ref. 7). The location of the maximum open-mode stress point will migrate toward the middle surface of the curved beam as the beam depth decreases (ref. 1).

For a curved sandwich beam subjected to open-mode bending, however, the two face sheets tend to move apart from each other, and the induced open-mode stress distribution along the sandwich core depth direction is practically linear. The maximum and minimum open-mode stress points are located, respectively, at the inner and outer bonding interfaces between the sandwich core and face sheets (refs. 6, 7). This unfavorable location of the maximum open-mode stress point in the curved sandwich beam could be a potential debonding failure site if the open-mode bending moment is too strong.

When a circular cylindrical fuel tank with “honeycomb” sandwich walls is filled with cryogen, the inner face sheet will cool down and shrink, and its radius will decrease. The circumferential shrinking of the cooler inner face sheet will pull the core inward and induce open-mode stress in the sandwich core depth direction. If the tank is also subjected to internal pressure, the pressure loading will cause the tank wall to expand and, as a result, either mitigate, nullify, or reverse (tension into compression) the open-mode stress depending on the magnitude of the internal pressure. If the magnitude of the open-mode stress exceeds the interfacial bonding strength, interfacial debonding between the face sheets and sandwich core could occur. If the tensile failure strength of the core

material is weaker than the interfacial bonding strength, however, tensile failure will occur in the sandwich core instead of at the interface.

A lobed cryogenic tank recently was proposed for use in a generic spacecraft. The tank is fabricated with honeycomb core sandwich walls and consists of two "eclipsed" (partially flattened) circular cylinders joined together at the eclipsed flat regions to form a common wall. The lobed cross section can be described as a D-shaped geometry joined together with its mirror image at the vertical lines.

Under internal pressure and cryogenic cooling, this type of lobed tank wall will experience open-mode and shear stress concentrations at the junctures where curved wall changes into flat wall (known as a curve-flat juncture). The debonding failure caused by excess open-mode or shear stresses actually was observed in a recent structural integrity test of such type of cryogenic tank. This incident motivated careful analysis of the structural performance of this type of lobed tank.

This report presents a finite-element debonding stress concentration analysis of the lobed fuel tank subjected to internal pressure and cryogenic cooling and shows that destructive open-mode and shear stress concentrations can be induced in the honeycomb core at the curve-flat juncture sites. A simple method to overcome the debonding stress concentration problems in the lobed honeycomb sandwich cryogenic tank is discussed.

LOBED SANDWICH TANK

Figure 1 shows the cross-sectional shape of the lobed cryogenic tank fabricated with honeycomb core composite sandwich walls. The lobed tank consists of two eclipsed obtuse circular cylinders (D-shaped, radius a = 84 in.) joined together at the eclipsed flat regions to form a common flat double wall. The centers of the two eclipsed circles are separated by a distance of $2l$ = 72 in. The inner laminated composite face sheet (13-ply) has a thickness t_1 = 0.066 in., and the outer laminated composite face sheet (7-ply) has a thickness t_2 = 0.034 in. The Korex® (E.I. du Pont de Nemours and Company, Wilmington, Delaware) honeycomb core (cell size d = 3/16 in., cell wall thickness t_w = 0.004 in., density $\rho_{hc} = 1.7360 \times 10^{-3}$ lb/in^3) has a depth h = 1.5 in. The inner face sheet was cooled down to a cryogenic temperature $T_1 = -423$ °F, and the outer face sheet remained at a room temperature T_2 = 70 °F. The tank was also subjected to an internal pressure p = 42 lb/in^2.

DESCRIPTION OF THE PROBLEM

Because the D-shaped geometry of the unit tank is nonaxisymmetric, the internal pressure p will bend the tank wall into a noncircular arc shape, causing open-mode and shear stress concentrations to arise at the curve-flat junctures. Also, the cryogenic cooling and consequent circumferential shrinking of the inner face sheet will reinforce the stress concentrations. The combined effect could induce high levels of open-mode and shear stress concentrations in the sandwich core at the curve-flat juncture and cause debonding failure.

The open-mode and shear failure stresses of the Korex® honeycomb core sandwich panel are quite low as shown in table 1. For comparison, the debonding strengths of other types of sandwich panels are presented in the appendix (refs. 8, 9). Therefore, the curve-flat juncture site, which is a high open-mode and shear stress concentration zone, could be the potential debonding failure site.

Table 1. Average failure strengths of Korex® honeycomb core sandwich panels.

Failure location	Face-wise tensile strength, lb/in^2	Shear strength, lb/in^2
Core	550*	115–220**
Core-adhesive interface	268*	--------

* Unpublished test data by T. H. Hou and N. J. Johnston, NASA Langley Research Center (Hampton, Virginia).

** Manufacturer's data.

The problem is to conduct a finite-element stress analysis of the lobed cryogenic tank and examine the levels of open-mode and shear stress concentrations induced in the honeycomb tank wall. The study also compares the levels of component contributions from internal pressure and temperature loading to the open-mode and shear debonding failure.

A case in which the honeycomb core at the curve-flat juncture region (3 in. long from the corner in each direction) is replaced locally with laminated composite (solid core) is analyzed to examine the change in open-mode and shear debonding stress concentrations. Additionally, the structural performance of the trivial case of a circular cylindrical honeycomb sandwich tank is examined.

FINITE-ELEMENT ANALYSIS

This section discusses the finite-element analysis. Finite-element modeling, constraint conditions, loading conditions, and the cell wall stress calculations are described in detail.

Finite-Element Modeling

The SPAR (Structures Performance And Resizing) finite-element computer program (ref. 10) was used in the finite-element analysis. Because of symmetry, only one-quarter of the tank cross section was modeled (two-dimensional modeling). Figure 2 shows the one-quarter model with unit thickness in the cylinder axial direction. The E41 (quadrilateral membrane elements) and E31 (triangular membrane elements) with unit thickness were used to model the composite face sheets and the honeycomb core. Both the face sheets and sandwich core were represented with equivalent continuous orthotropic materials. Each face sheet was modeled with one layer of E41 elements, and the honeycomb core was modeled with eight layers of E41 and E31 elements. Table 2 lists the size of the one-quarter model of the lobed fuel tank cross-sectional segment.

Table 2. Size of one-quarter finite-element model of the lobed fuel tank.

Item	Number
JLOC	3,241
E41 elements	2,932
E31 elements	4

Constraint Conditions

In the curved region, the nodes lying in the symmetry plane (*x*-*z* plane) were allowed to move freely only in the *x*-direction, but they were constrained to have no tangential motions and no rotations about the *z*-axis to simulate the conditions at the symmetry plane. In the flat region, the bonded flat outer face sheets were allowed to move only in the *y*-direction (no *x*-displacements).

Loading Conditions

For pressure loading, the internal pressure *p* was converted into radial nodal force F_i at the inner surface node *i* through

$$F_i = p\left|\frac{s_{(i+1)-i} + s_{i-(i-1)}}{2}\right| \times 1 \tag{1}$$

where $s_{(i+1)-i}$ and $s_{i-(i-1)}$ are, respectively, the curve lengths between the inner surface nodes $(i + 1)$ and *i*, and between the inner surface nodes *i* and $(i - 1)$.

If the surface node was located at the symmetry plane (that is, the *x*-*z* plane), then $F_i/2$ was used instead of F_i. When the surface node was located at the curve-flat juncture point, one-half of the curved region nodal force F_i was directed in the radial direction, and one-half of the flat region nodal force F_j was directed in the *x*-direction. The flat region nodal force F_j is not exactly the same as the curved region nodal force F_i, because the finite-element mesh sizes at the curved and flat regions are slightly different.

For temperature loading, a temperature $T_1 = -423$ °F was applied at every inner face sheet node, and a temperature $T_2 = 70$ °F was applied at every outer face sheet node. For temperature loading at the sandwich core nodes (8 layers of E41 elements), a linear temperature distribution was used.

Cell Wall Stresses

The finite-element analysis computes the effective radial stress σ_r for the honeycomb core. The actual radial stress induced in the honeycomb cell wall σ_w can be calculated from

$$\sigma_w = \frac{A_c}{A_w}\sigma_r = \frac{\rho_c}{\rho_{hc}}\sigma_r \tag{2}$$

where A_c and A_w are, respectively, the cross-sectional areas (normal to the honeycomb cell generatrix) of the unit honeycomb cell and cell wall; ρ_c is the density of the honeycomb core material; and ρ_{hc} is the effective density of the honeycomb core structure.

For an ideal right hexagonal honeycomb cell, the area ratio A_c/A_w can be expressed as (ref. 11)

$$\frac{A_c}{A_w} = \frac{3\sqrt{3}}{16}\frac{d}{t_w} \tag{3}$$

where *d* is the cell size (maximum diagonal of the cell cross section), and t_w is the cell wall thickness.

For the common hexagonal honeycomb cell (in which the two opposite sides bonded to the neighboring cells are slightly shorter than the remaining four sides), the area ratio A_c/A_w can be expressed as (ref. 11)

$$\frac{A_c}{A_w} = \frac{15}{112}(3\sqrt{2}-2)\frac{d}{t_w} \tag{4}$$

Thus, equation (2) takes the following forms:

For the right hexagonal cell,

$$\sigma_w = \frac{A_c}{A_w}\sigma_r = \frac{3\sqrt{3}}{16}\frac{d}{t_w}\sigma_r \tag{5}$$

For the common hexagonal cell,

$$\sigma_w = \frac{A_c}{A_w}\sigma_r = \frac{15}{112}(3\sqrt{2}-2)\frac{d}{t_w}\sigma_r \tag{6}$$

For the current honeycomb core with a cell size *d* = 3/16 in. and an approximate cell wall thickness t_w = 0.004 in., the area ratios are A_c/A_w = 15.2231 for the right hexagonal cell, and A_c/A_w = 14.0791 for the common hexagonal cell. Then the stress equations (5) and (6) become

$$\sigma_w = \frac{A_c}{A_w}\sigma_r = 15.2231\sigma_r \tag{7}$$

$$\sigma_w = \frac{A_c}{A_w}\sigma_r = 14.0791\sigma_r \tag{8}$$

Equations (7) and (8) show that the value of the actual cell wall stress σ_w is enhanced by 14–15 times that of the effective radial stress σ_r. A similar argument is applicable to the flat region.

RESULTS

This section discusses the deformations and stress concentrations in the lobed honeycomb composite sandwich tank. Deformations, open-mode stresses, core shear stresses, failure loads, tangential stresses, and the solid curve-flat juncture are described in detail. A circular cylindrical sandwich composite tank also is analyzed.

Deformations

Figure 3 shows the deformed shape of the fuel tank under internal pressure loading only (referred to as "*p*-only" loading). Because of nonaxisymmetrical loading, the curved region bulged outward in the horizontal direction with a displacement of δ_r = 1.20836 in. along the *x*-axis. The curve-flat juncture corner moved outward by δ_y = 0.11243 in.

Figure 4 shows the deformed shape of the lobed tank under temperature loading only (referred to as "*T*-only" loading). The curve-flat juncture corner moved inward (downward) by δ_y = – 0.03420 in. because of shrinking of the flat region. The wall at the *x*-axis moved slightly outward, however, by δ_r = 0.06945 in., which is approximately 6 percent of the *p*-only loading case. Because of the anisotropic nature of the face sheets and the core, not every point of the tank wall moved inward from the undeformed position. If the materials were set to be isotropic, the deformed shape was found to lie inside the undeformed shape without intersecting the latter.

Figure 5 shows the deformed shape of the lobed tank under combined internal pressure and temperature loading (referred to as "$p + T$" loading). Because the pressure loading dominates the temperature loading, the deformed shape in the combined loading case looks similar to that in the pressure loading case (fig. 3), with a wall horizontal displacement of δ_r = 1.27781 (1.20836 + 0.06945) in. The curve-flat juncture corner moved outward with a displacement of δ_y = 0.07823 (0.11243 – 0.03420) in. Table 3 presents the displacements at typical points of the tank wall.

Table 3. Displacements at typical points of composite sandwich lobed tank wall.

Loading	δ_r, in.	δ_y, in.
p-only	1.20836	0.11243
T-only	0.06945	– 0.03420
$p + T$	1.27781	0.07823

Open-Mode Stresses

Figures 6–8 show tangential distributions of open-mode stresses at the inner bonding interface, which is the critical interface. Under *p*-only loading (fig. 6), the sandwich core is under compression in the curved and flat regions and turned to sever tension in the curve-flat juncture with a maximum open-mode stress of σ_r = 1,288 lb/in^2. This stress level far exceeds the open-mode strength of the core shown in table 1. Therefore, under internal pressure (p = 42 lb/in^2) only, the tank wall will fail through open-mode debonding at the inner interface of the curve-flat juncture.

Under *T*-only loading (fig. 7), the core in the curved region is under very small tension, but the core in the flat region is under infinitesimal compression. The maximum open-mode stress is only σ_r = 222 lb/in^2, which is slightly lower than the open-mode failure strength of the core (table 1). Therefore, cryogenic cooling alone will not cause open-mode failure.

The open-mode stress distribution in the $p + T$ loading case (fig. 8) is very similar to that in the *p*-only loading case but has a higher maximum open-mode stress of σ_r = 1,490 lb/in^2, which is the summation of the other two cases. The calculated open-mode stress of σ_r = 1,490 lb/in^2 far exceeds the open-mode strength of the sandwich core (table 1). Therefore, under the present combined loading condition, the open-mode debonding failure is inevitable at the curve-flat juncture of the lobed sandwich tank.

Figure 9 shows the distribution of open-mode stresses σ_r across the core depth at the curve-flat juncture under combined internal pressure and temperature loading. The distribution of σ_r along the core depth direction at the curve-flat juncture is nonlinear and concave upward. This σ_r distribution is different from that in the curved sandwich bar cases (refs. 6, 7) in which the distribution of σ_r along the core depth direction is practically linear with a very small slope. At the curve-flat juncture, the maximum value of σ_r (1,490 lb/in^2) at the inner bonding interface is approximately 3.49 times the minimum value of σ_r (427 lb/in^2) at the outer bonding interface in the $p + T$ loading case. The contributions from *p*-only and *T*-only loading are, respectively, 86.44 and 13.56 percent of the total open-mode stress value.

Core Shear Stresses

Figures 10–12 show tangential distributions of shear stresses induced in the honeycomb core. Under *p*-only loading (fig. 10), similar to the open-mode case, the severe core shear stress concentration occurs at the curve-flat juncture with a maximum shear stress of $\tau_{r\theta}$ = 662 lb/in^2, which exceeds the shear strength of the core (table 1). Therefore, under internal pressure alone (that is, p = 42 lb/in^2), the tank will certainly fail in shear at the curve-flat juncture site.

Under *T*-only loading (fig. 11), the maximum core shear stress is only $\tau_{r\theta}$ = 105 lb/in^2 at the curve-flat juncture and is slightly lower than the lowest shear failure stress of 115 lb/in^2 (table 3). Thus, the tank wall is unlikely to suffer shear failure under cryogenic cooling alone (T_1 = – 423 °F).

The core shear stress distribution in the $p + T$ loading case (fig. 12) is very similar to that in the *p*-only loading case. The maximum core shear stress $\tau_{r\theta}$ = 767 lb/in^2 (the summation of the pressure and temperature loading cases) is located at the curve-flat juncture and is 3.49 times greater than the upper bound of the shear failure stress (table 1).

Figure 13 shows the distribution of core shear stresses $\tau_{r\theta}$ across the core depth at the curve-flat juncture under combined internal pressure and temperature loading. The distribution of $\tau_{r\theta}$ along the core depth direction at the curve-flat juncture is nonlinear and concave upward, similar to that in the open-mode case (fig. 9). The maximum value of $\tau_{r\theta}$ (767 lb/in^2) at the inner bonding interface of the curve-flat juncture in the $p + T$ loading case is approximately 3.62 times the minimum value of $\tau_{r\theta}$ (212 lb/in^2) at the outer bonding interface. In the core shear case, the relative contributions from internal pressure and temperature loading are, respectively, 86.31 and 13.69 percent.

Failure Loads

The analysis discussed in the previous section shows that the honeycomb core sandwich lobed tank wall will certainly fail in both open-mode and shear-mode debonding under the *p*-only and $p + T$ loading conditions (table 1). Table 4 tabulates the results of the failure modes.

Table 4. Summary of maximum core stresses at curve-flat juncture.

Loading	σ_r, lb/in^2	Open-mode failure	$\tau_{r\theta}$, lb/in^2	Shear failure
p-only	1,288	yes	662	yes
T-only	202	no	105	no
$p + T$	1,490	yes	767	yes

Assuming that the values of the open-mode and core shear stress increase linearly with the increasing of load, one can calculate, from the following equations, the exact loading levels at which failure (open-mode or shear) initiates.

For pressure load:

$$\text{Failure pressure} = \frac{\text{Failure stress}}{\text{Maximum stress}} \times 42 \ \ (\text{lb/in}^2) \tag{9}$$

For temperature load:

$$\text{Failure temperature} = \left[- \frac{\text{Failure stress}}{\text{Maximum stress}} \times (423 + 70) + 70 \right] (^\circ\text{F}) \tag{10}$$

Tables 5 and 6 summarize the failure loads calculated from equations (9) and (10). As shown, under very small internal pressures, the honeycomb sandwich-walled lobed tank will fail in both open-mode and shear-mode debonding.

Table 5. Estimated internal pressure for debonding failures; *p*-only loading.

Loading	Open-mode failure pressure, lb/in^2	Shear-mode failure pressure, lb/in^2
p-only	8.72	17.00

Table 6. Estimated temperatures for debonding failures; *T*-only loading.

Loading	Open-mode failure temperature, °F	Shear-mode failure temperature, °F
T-only	– 584.08*	– 469.95*

* Lower than the applied temperature T_1 = – 423 °F; that is, no failure.

Tangential Stresses

Figures 14 and 15 show tangential distributions of tangential stresses $\{\sigma_\theta, \sigma_y\}$ in the inner face sheet, respectively, under *p*-only and *T*-only loading. The tangential stress σ_θ is positive (tension) everywhere. The effect of *p*-only loading is approximately 8.66 times greater than that of *T*-only loading. In the *p*-only loading case (fig. 14), σ_θ is maximum (σ_θ = 33,336 lb/in^2) at the horizontal axis of symmetry (*x*-axis) and gradually decreases toward the curve-flat juncture. Beyond the curve-flat juncture, σ_θ changes to σ_y, increases again, becomes almost constant as the *x*-axis is approached, and reaches a value of σ_y = 14,699 lb/in^2 on the *x*-axis. In the inner face sheet, the maximum tangential stress (σ_y = 14,699 lb/in^2) induced in the flat region is roughly 44 percent of the maximum tangential stress (σ_θ = 33,336 lb/in^2) induced in the curved region. In the *T*-only loading case (fig. 15), the maximum tangential stress (σ_y = 4,163 lb/in^2) induced in the flat region is approximately 1.08 times the maximum tangential stress (σ_θ = 3,851 lb/in^2) induced in the curved region.

Figures 16 and 17 show tangential distributions of tangential stresses $\{\sigma_\theta, \sigma_y\}$ in the outer face sheet, respectively, under *p*-only and *T*-only loading. The effect of *p*-only loading (fig. 16) is far greater than that of *T*-only loading (fig. 17).

In the *p*-only loading case, the tangential stresses $\{\sigma_\theta, \sigma_y\}$ are positive (tension) everywhere. The tangential stress σ_θ (38,447 lb/in^2 on the *x*-axis) gradually increases from the *x*-axis and reaches a maximum value (σ_θ = 77,831 lb/in^2) at the curve-flat juncture point. In the flat region, the tangential stress σ_y is maximum (σ_y = 30,599 lb/in^2) at the curve-flat juncture point and gradually decreases to σ_y = 14,466 lb/in^2 on the *x*-axis.

In the *T*-only loading case, the tangential stresses $\{\sigma_\theta, \sigma_y\}$ are negative (compression) everywhere. The maximum tangential compressive stress (σ_y = – 8,132 lb/in^2) in the flat region is approximately 1.10 times the magnitude of the tangential compressive stress (σ_θ = – 7,419 lb/in^2) induced in the curved region.

Figures 18 and 19 respectively show the tangential stresses $\{\sigma_\theta, \sigma_y\}$ induced in the inner and outer face sheets under $p + T$ loading. These stresses $\{\sigma_\theta, \sigma_y\}$ are the summation of component stresses $\{\sigma_\theta, \sigma_y\}$ (due to *p*) and $\{\sigma_\theta, \sigma_y\}$ (due to *T*). The stress values at critical points are indicated in the figures.

For the inner face sheet (fig.18), the tangential tensile stresses $\{\sigma_\theta, \sigma_y\}$ reach their respective maximum values at the *x*-axis. Conversely, for the outer face sheet (fig. 19), the tangential tensile stresses $\{\sigma_\theta, \sigma_y\}$ reach their respective maximum values at the curve-flat juncture.

Solid Curve-Flat Juncture

Figures 20–22 show the deformed shapes of the lobed tank when the honeycomb core in the vicinity of the curve-flat juncture was replaced with laminated composite (solid corner). These deformed shapes are similar to the corresponding deformed shapes in the honeycomb core cases (figs. 3–5). Table 7 lists the values of the tank wall displacements. Data from the honeycomb corner cases are shown in parentheses for comparison. Note that the values of δ_r increase, but the values of δ_y, except in the *T*-only loading case, decrease.

Table 7. Summary of displacements at typical points of the composite sandwich lobed tank wall; solid corner.

Loading	δ_r, in.	δ_y, in.
p-only	1.30909	0.08960
	(1.20836)	(0.11243)
T-only	0.10522	– 0.04039
	(0.06945)	(– 0.03420)
p + *T*	1.41431	0.04921
	(1.27781)	(0.07823)

( ) Honeycomb corner

Figures 23 and 24 respectively show distributions of open-mode stress σ_r and shear stress $\tau_{r\theta}$ across the solid core depth at the curve-flat juncture under three types of loading. Unlike in the honeycomb core cases (figs. 9, 13), the peak open-mode and shear stresses under *p*-only and *p* + *T* loading migrate to the outer interface. In the shear stress plots (fig. 24), the *p* + *T* and *p*-only loading curves intersect near the outer interface. Table 8 lists the maximum core stresses at the solid curve-flat juncture.

Table 8. Summary of maximum core stresses at solid curve-flat juncture.

Loading	σ_r, lb/in^2	$\tau_{r\theta}$ lb/in^2
p-only	2,419	877
	(1,288)	(662)
T-only	588	135
	(202)	(105)
p + *T*	3,007	1,012
	(1,490)	(767)

( ) Honeycomb corner

The open-mode debonding stresses at the curve-flat junctures practically double in the solid core case. In the *p* + *T* loading case, however, the open-mode stress σ_r = 3,007 lb/in^2 is only 60 percent of the delamination strength, 5,000 lb/in^2, of most of the composite materials (ref. 8).

Circular Cylindrical Tank

For comparison of structural performance, a circular cylindrical sandwich composite tank with the same radius as that of the lobed tank also was analyzed. Figures 25–27 show the axisymmetric deformed shapes, respectively, for the *p*-only, *T*-only, and *p* + *T* loading cases. Table 9 lists the radial displacements and debonding stresses.

Table 9. Stresses and displacements induced in a circular cylindrical sandwich composite tank.

Loading	δ_r, in.	σ_r, lb/in^2	$\tau_{r\theta}$, lb/in^2
p-only	0.2437	– 13.93	0
T-only	– 0.0456	3.28	0
p + *T*	0.1981	– 10.65	0

Notice from table 9 that, because of axisymmetry, the core shear stress $\tau_{r\theta}$ is zero. The open-mode stresses σ_r in the *p*-only and *p* + *T* loading cases are negative (compression). The *T*-only loading case induces negligible open-mode stress. As table 9 illustrates, debonding between the core and face sheets cannot occur in the circular composite sandwich tank.

CONCLUDING REMARKS

A finite-element debonding stress concentration analysis was performed on a composite “honeycomb” sandwich tank subjected to internal pressure (p = 42 lb/in^2) and cryogenic cooling (T_1 = – 423 °F). The primary findings of this analysis are as follows:

1. Intense open-mode and shear stress concentrations occurred at the curve-flat juncture site.
2. The effect of internal pressure loading on the open-mode and shear debonding stress concentrations was far greater than that of temperature loading.
3. Under internal pressure loading only, the lobed fuel tank failed in both open-mode and shear debonding.
4. Under cryogenic cooling alone, the lobed fuel tank did not fail in both open-mode and shear debonding.
5. Under combined internal pressure loading and cryogenic cooling, the lobed fuel tank failed in both open-mode and shear debonding at a very low level of loading.
6. The lobed fuel tank with honeycomb sandwich walls was found to be incapable of carrying a sufficient internal pressure load, because the lobed geometry created intense open-mode and shear stress concentrations at the curve-flat juncture.
7. If the honeycomb core at the curve-flat juncture were replaced with a composite solid core, the open-mode stress could be reduced below the composite delamination strength, and thus the debonding failure problem could be eliminated.
8. In the circular cylindrical sandwich tank, the debonding problem did not exist because of axisymmetry.

Dryden Flight Research Center
National Aeronautics and Space Administration
Edwards, California
September 30, 2003

FIGURES

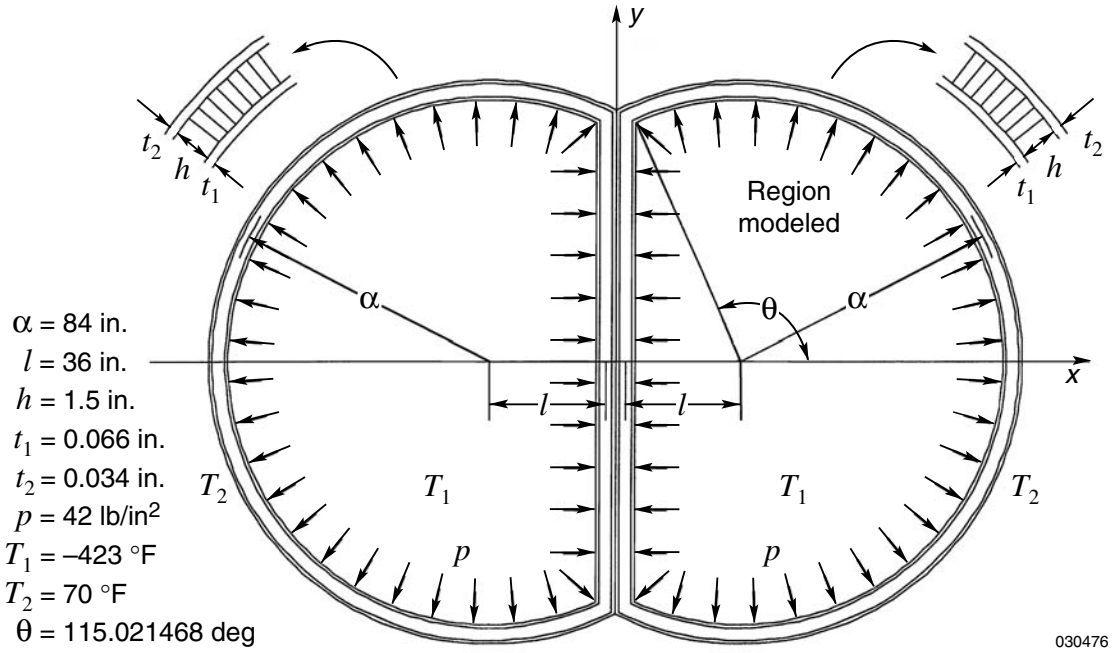

Figure 1. Cross section of lobed cryogenic tank with honeycomb sandwich walls subjected to internal pressure and cryogenic cooling; p = 42 lb/in^2, T_1 = –423 °F, T_2 = 70 °F.

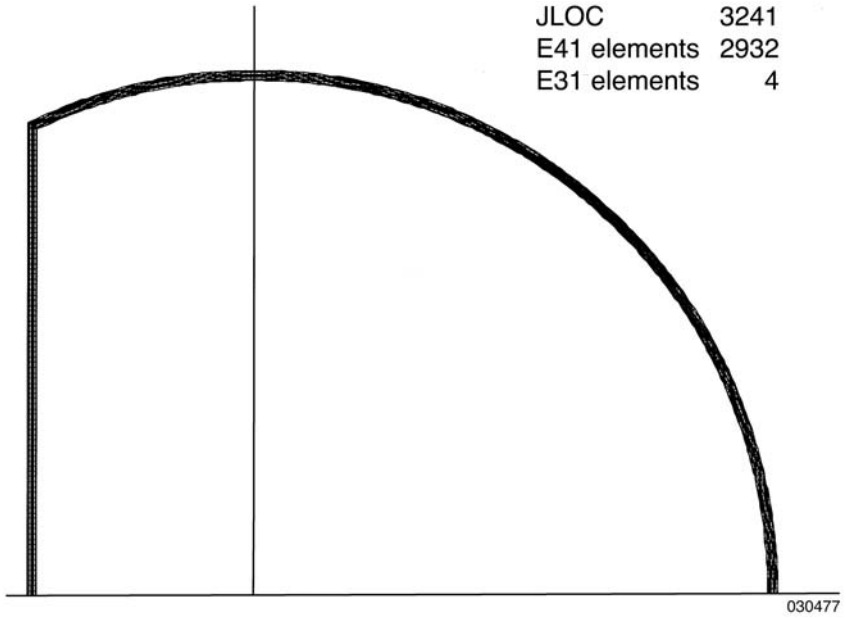

Figure 2. Finite-element model for the first quadrant of cryogenic tank.

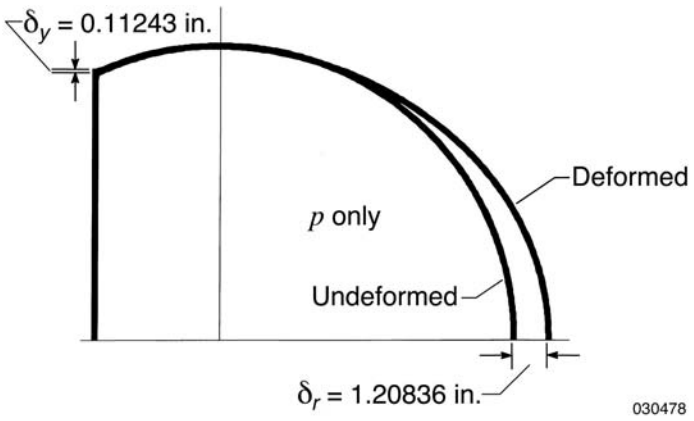

Figure 3. Deformed shape of sandwich composite cryogenic tank under internal pressure loading only; p = 42 lb/in^2.

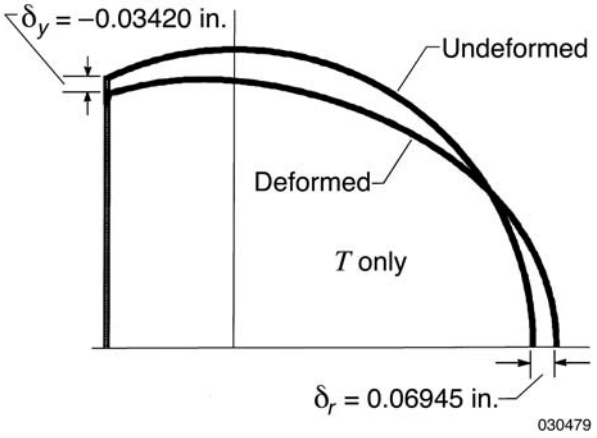

Figure 4. Deformed shape of sandwich composite cryogenic tank under temperature loading only; T_1 = −423 °F, T_2 = 70 °F.

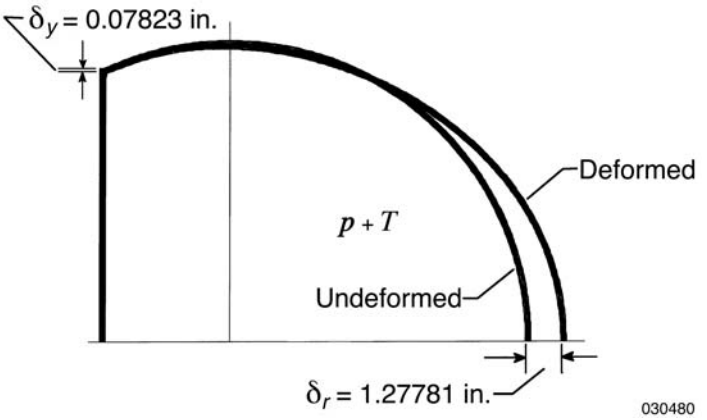

Figure 5. Deformed shape of sandwich composite cryogenic tank under combined internal pressure and temperature loading; p = 42 lb/in^2, T_1 = −423 °F, T_2 = 70 °F.

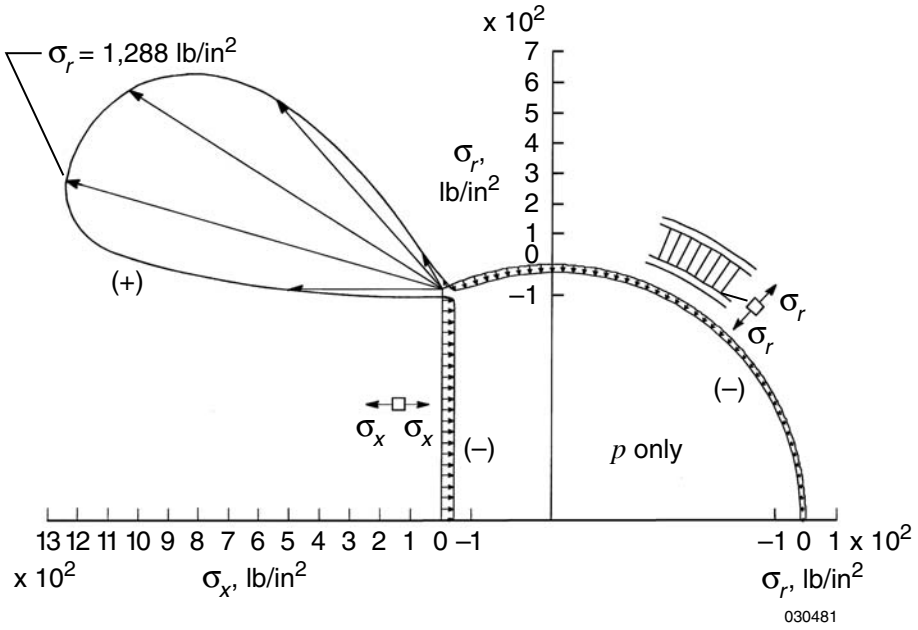

Figure 6. Tangential distribution of open-mode stresses $\{\sigma_r, \sigma_x\}$ at the inner bonding interface; internal pressure loading only; p = 42 lb/in^2.

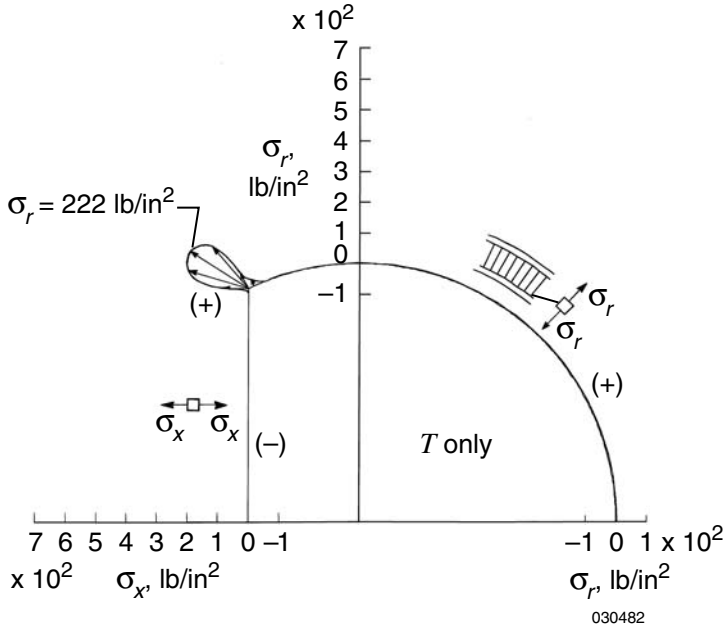

Figure 7. Tangential distribution of open-mode stresses $\{\sigma_r, \sigma_x\}$ at the inner bonding interface; temperature loading only; T_1 = –423 °F, T_2 = 70 °F.

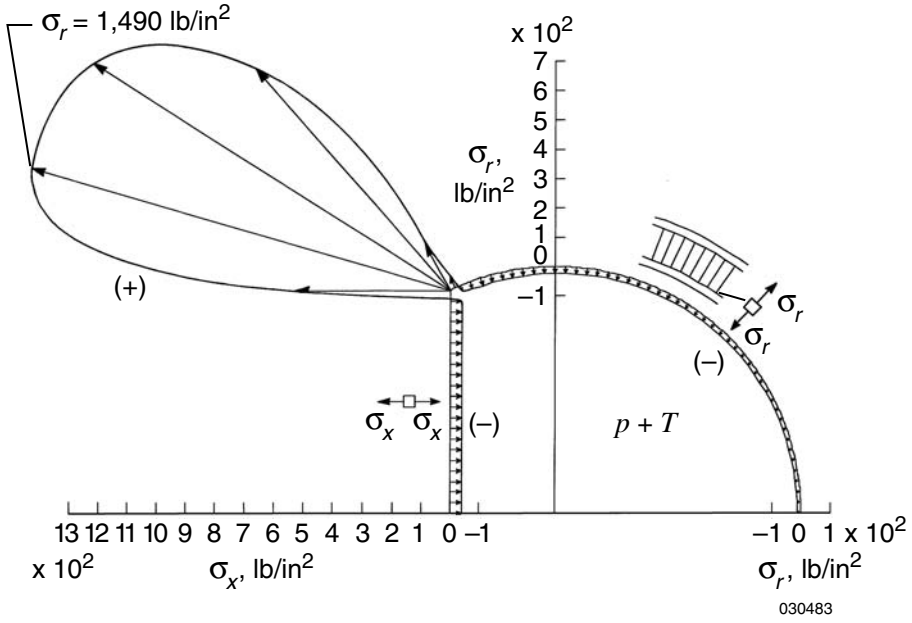

Figure 8. Tangential distribution of open-mode stresses $\{\sigma_r, \sigma_x\}$ at the inner bonding interface; combined internal pressure and temperature loading; p = 42 lb/in^2, T_1 = –423 °F, T_2 = 70 °F.

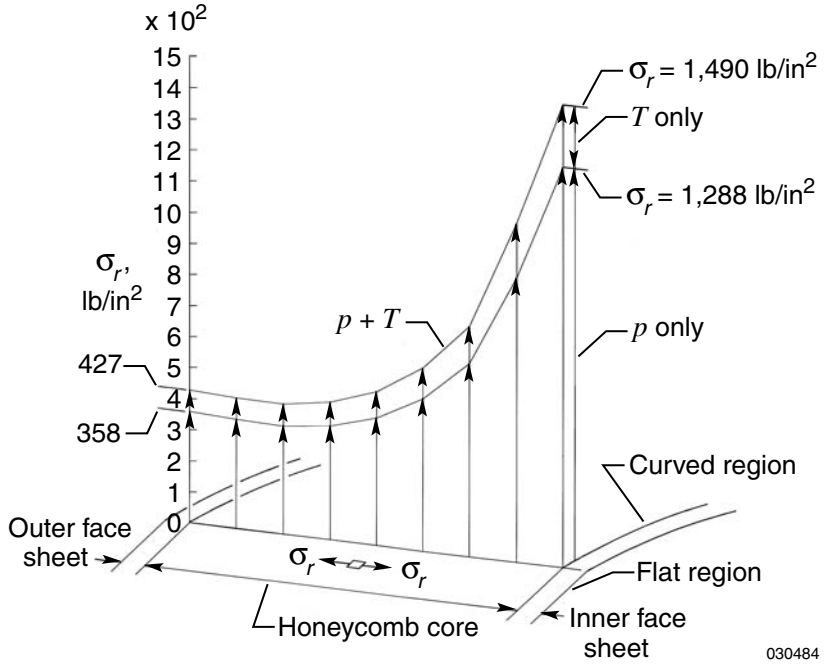

Figure 9. Radial distribution of open-mode stresses σ_r across the core depth at curve-flat juncture; combined internal pressure and temperature loading; p = 42 lb/in^2, T_1 = –423 °F, T_2 = 70 °F.

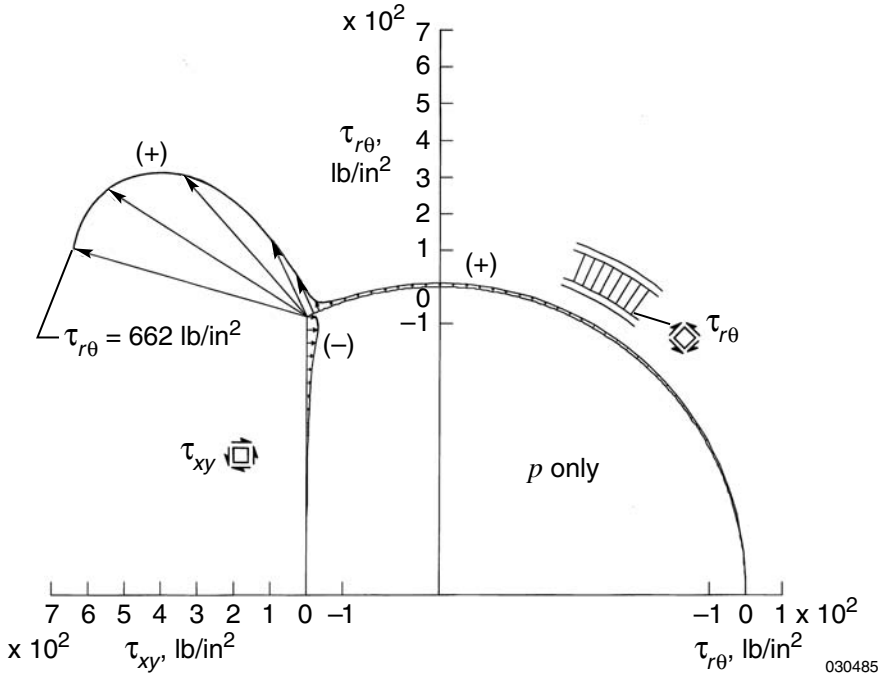

Figure 10. Tangential distribution of shear stresses $\{\tau_{r\theta}, \tau_{xy}\}$ at the inner bonding interface; internal pressure loading only; p = 42 lb/in^2.

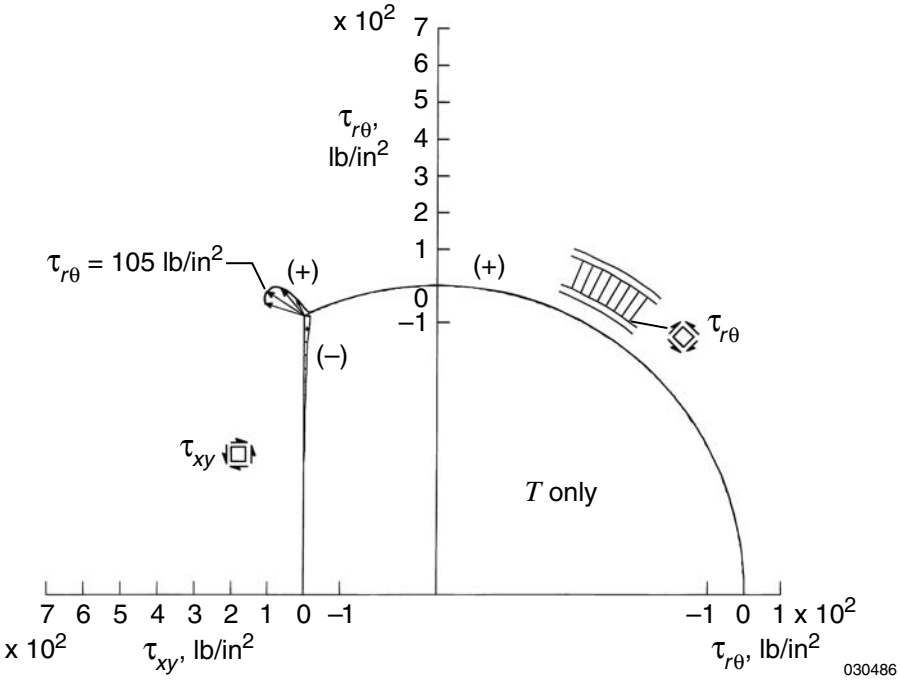

Figure 11. Tangential distribution of shear stresses $\{\tau_{r\theta}, \tau_{xy}\}$ at the inner bonding interface; temperature loading only; T_1 = –423 °F, T_2 = 70 °F.

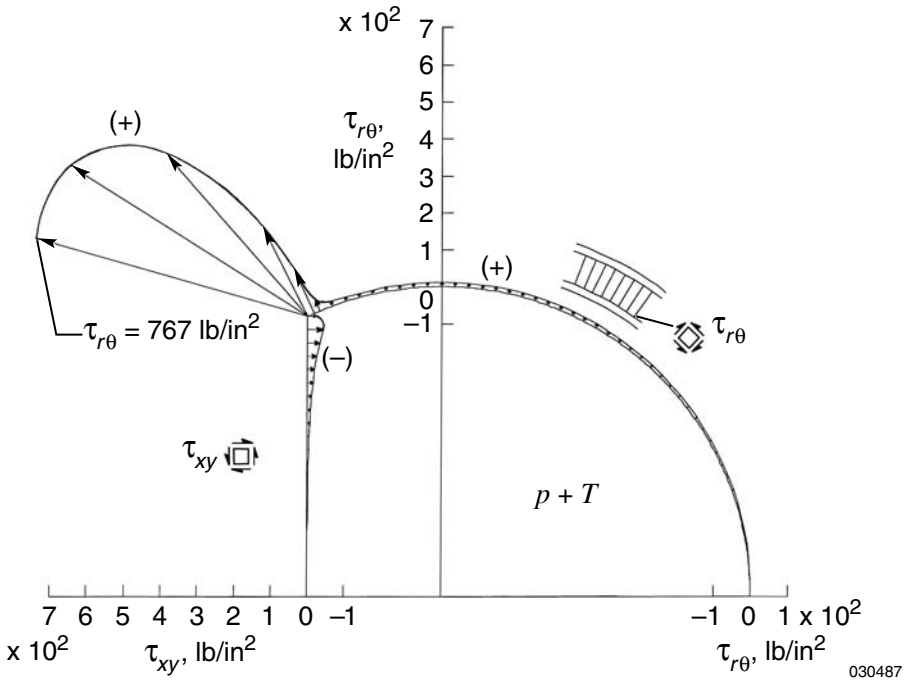

Figure 12. Tangential distribution of shear stresses $\{\tau_{r\theta}, \tau_{xy}\}$ at the inner bonding interface; combined internal pressure and temperature loading; p = 42 lb/in^2, T_1 = –423 °F, T_2 = 70 °F.

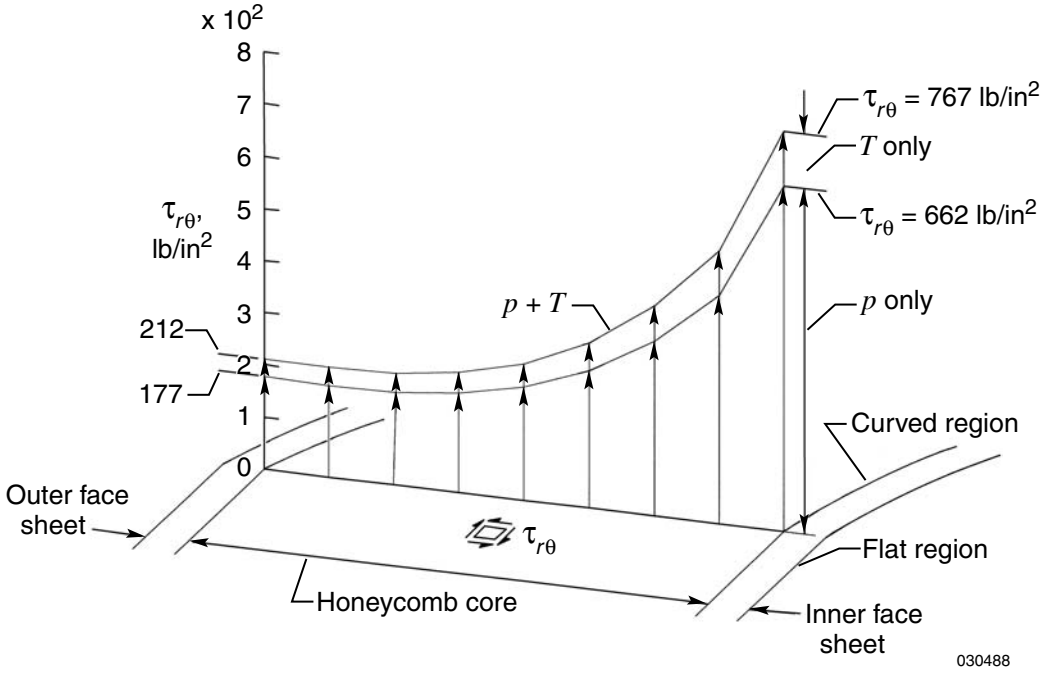

Figure 13. Radial distribution of shear stresses $\tau_{r\theta}$ across the core depth at curve-flat juncture; combined internal pressure and temperature loading; p = 42 lb/in^2, T_1 = –423 °F, T_2 = 70 °F.

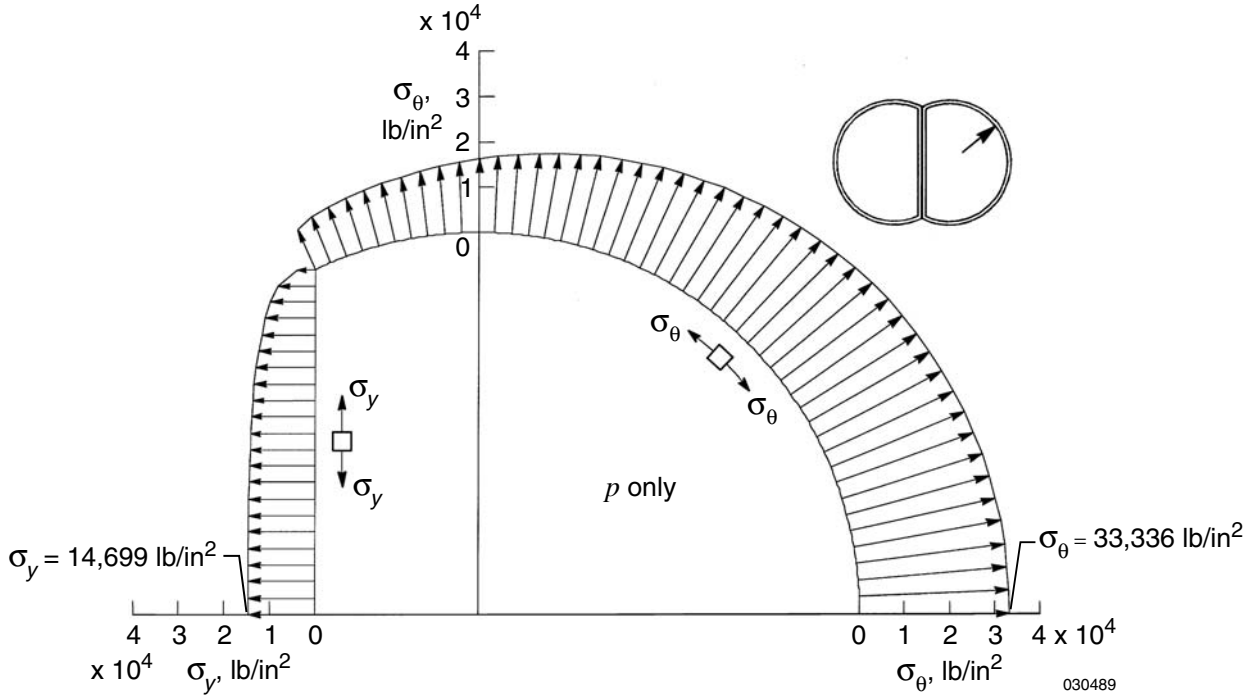

Figure 14. Tangential distribution of tangential stresses $\{\sigma_\theta, \sigma_y\}$ in the inner face sheet; internal pressure loading only; p = 42 lb/in^2.

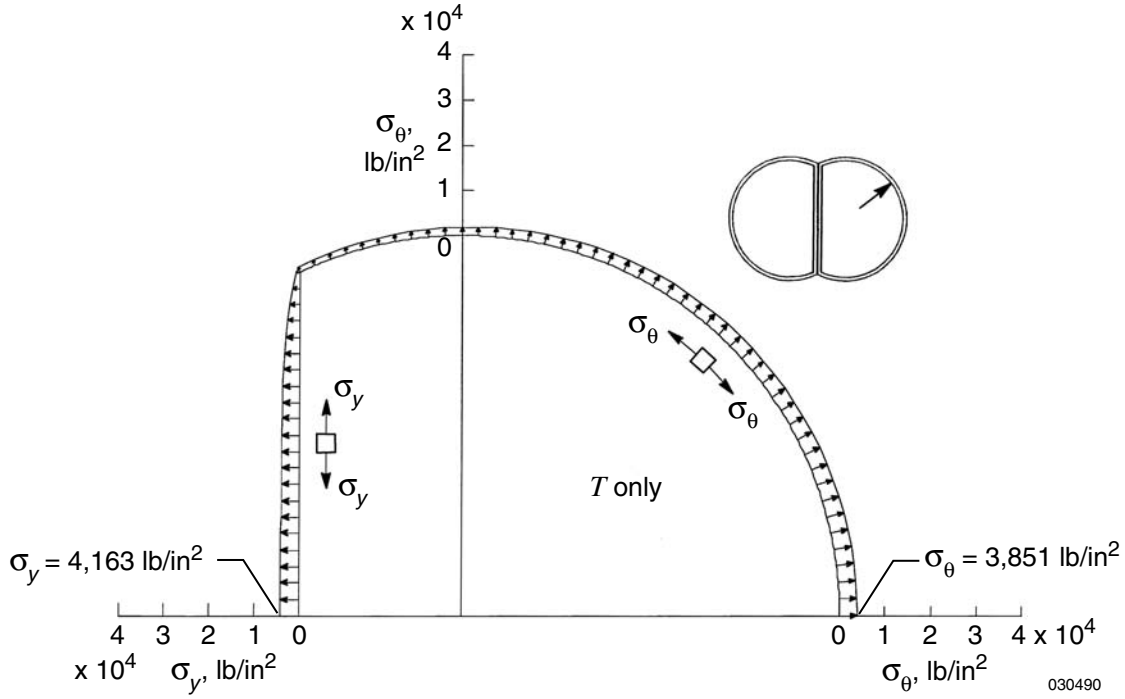

Figure 15. Tangential distribution of tangential stresses $\{\sigma_\theta, \sigma_y\}$ in the inner face sheet; temperature loading only; T_1 = –423 °F, T_2 = 70 °F.

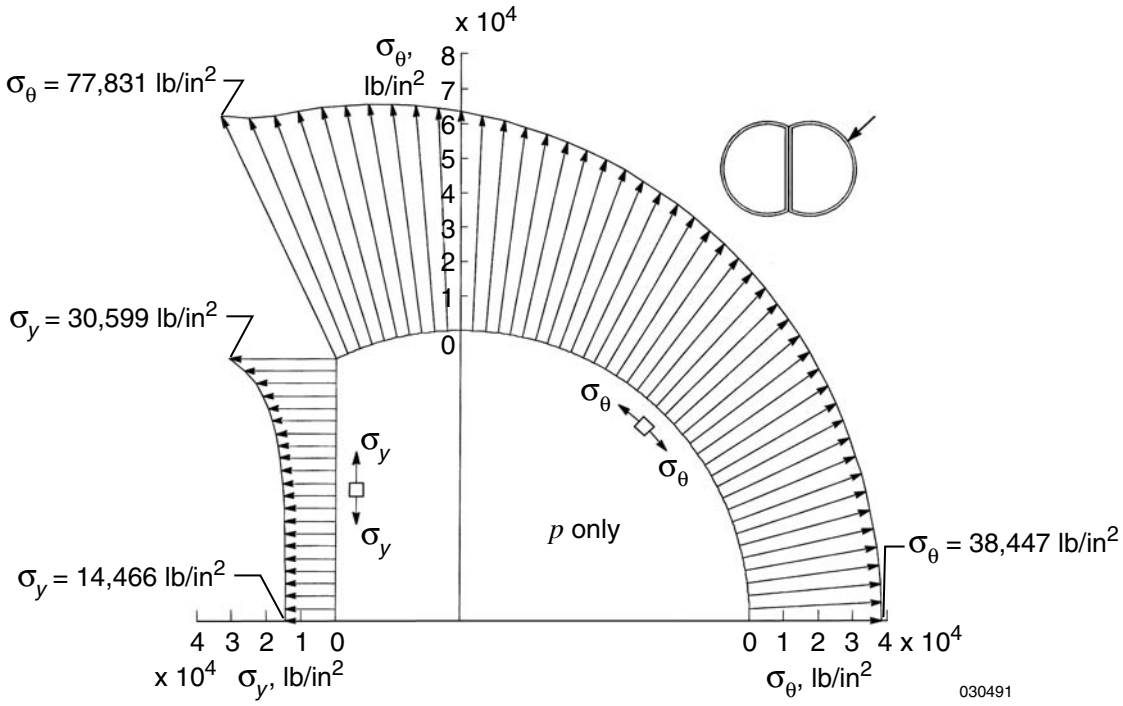

Figure 16. Tangential distribution of tangential stresses $\{\sigma_\theta, \sigma_y\}$ in the outer face sheet; internal pressure loading only; p = 42 lb/in^2.

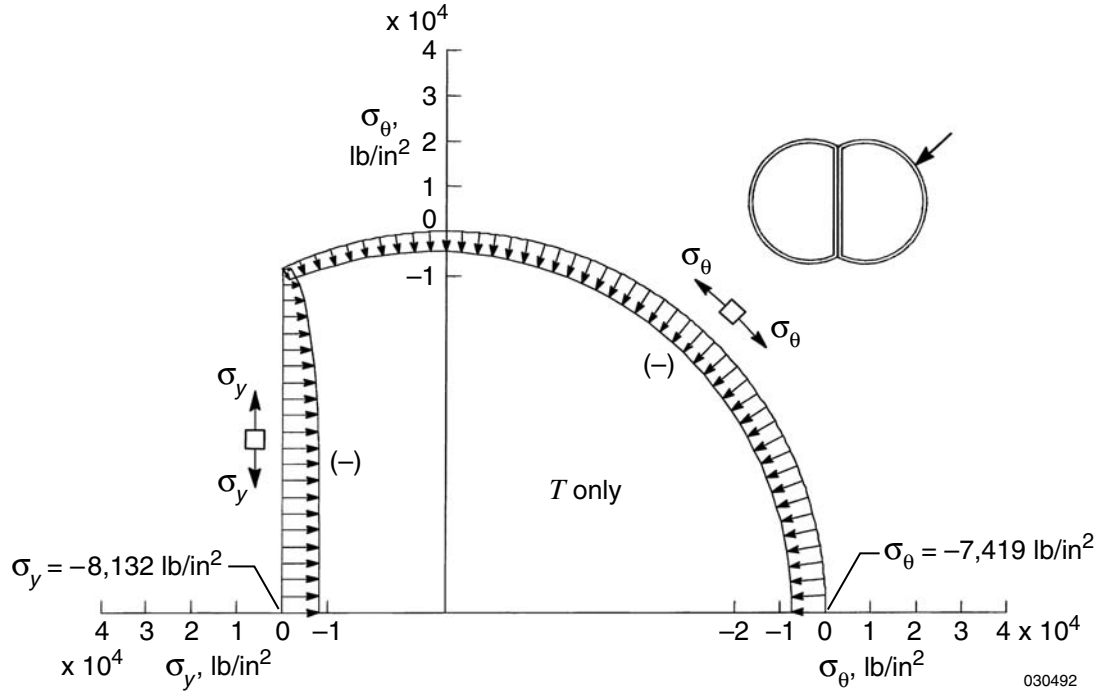

Figure 17. Tangential distribution of tangential stresses $\{\sigma_\theta, \sigma_y\}$ in the outer face sheet; temperature loading only; T_1 = −423 °F, T_2 = 70 °F.

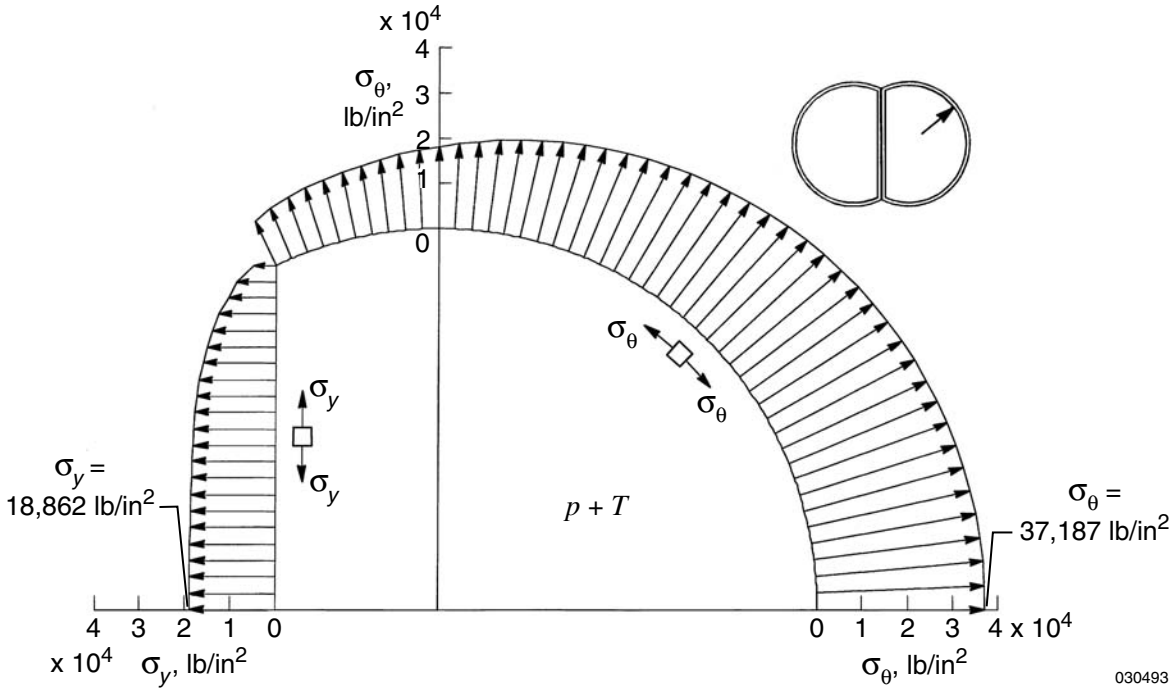

Figure 18. Tangential distribution of tangential stresses $\{\sigma_\theta, \sigma_y\}$ in the inner face sheet; combined internal pressure and temperature loading; p = 42 lb/in^2, T_1 = –423 °F, T_2 = 70 °F.

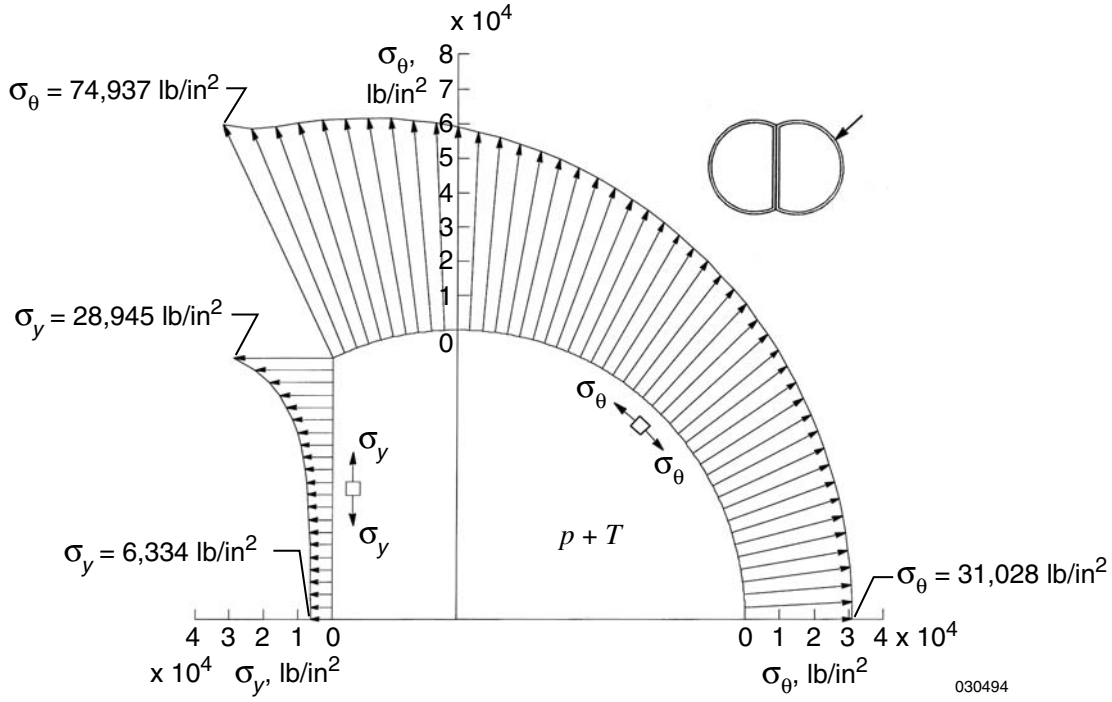

Figure 19. Tangential distribution of tangential stresses $\{\sigma_\theta, \sigma_y\}$ in the outer face sheet; combined internal pressure and temperature loading; p = 42 lb/in^2, T_1 = –423 °F, T_2 = 70 °F.

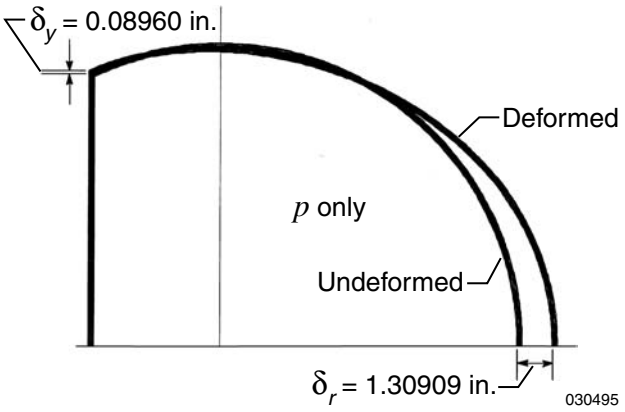

Figure 20. Deformed shape of sandwich composite cryogenic tank under internal pressure loading only; p = 42 lb/in^2; solid corner.

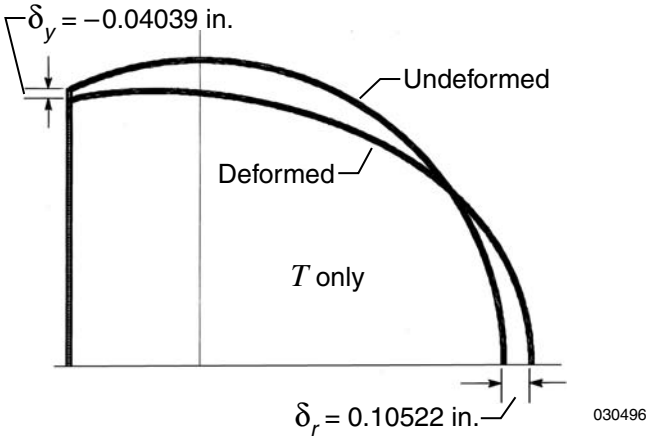

Figure 21. Deformed shape of sandwich composite cryogenic tank under temperature loading only; T_1 = −423 °F, T_2 = 70 °F; solid corner.

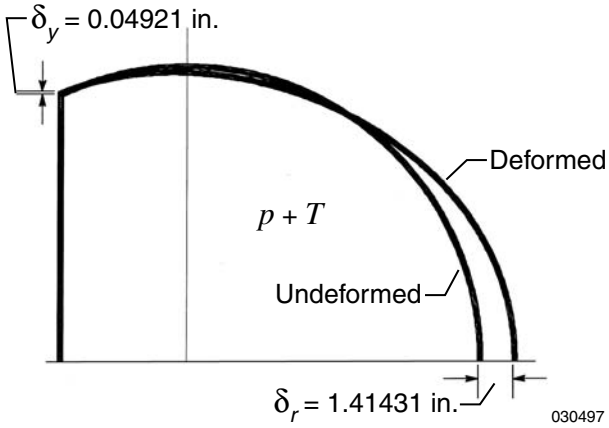

Figure 22. Deformed shape of sandwich composite cryogenic tank under combined internal pressure and temperature loading; p = 42 lb/in^2, T_1 = −423 °F, T_2 = 70 °F; solid corner.

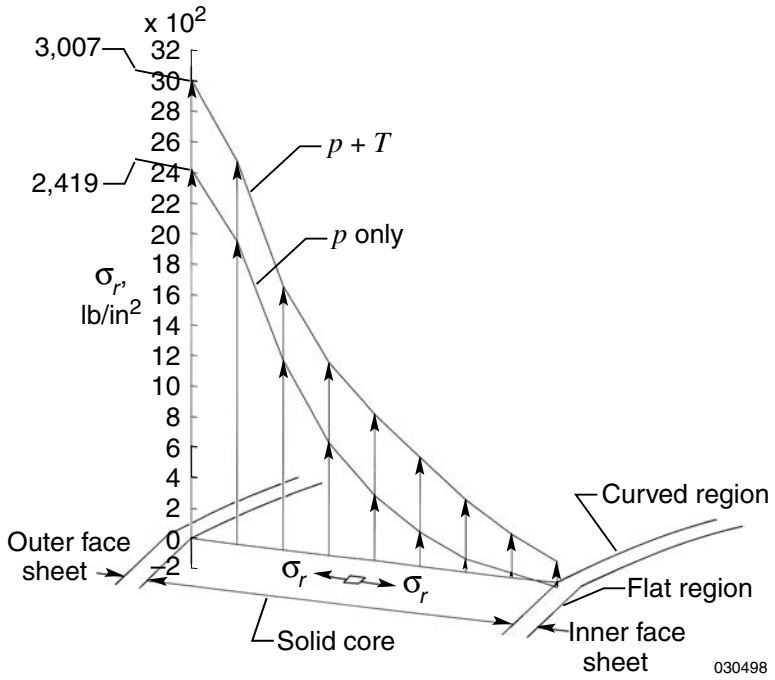

Figure 23. Radial distribution of open-mode stresses σ_r at curve-flat juncture; combined internal pressure and temperature loading; p = 42 lb/in^2, T_1 = –423 °F, T_2 = 70 °F; solid corner.

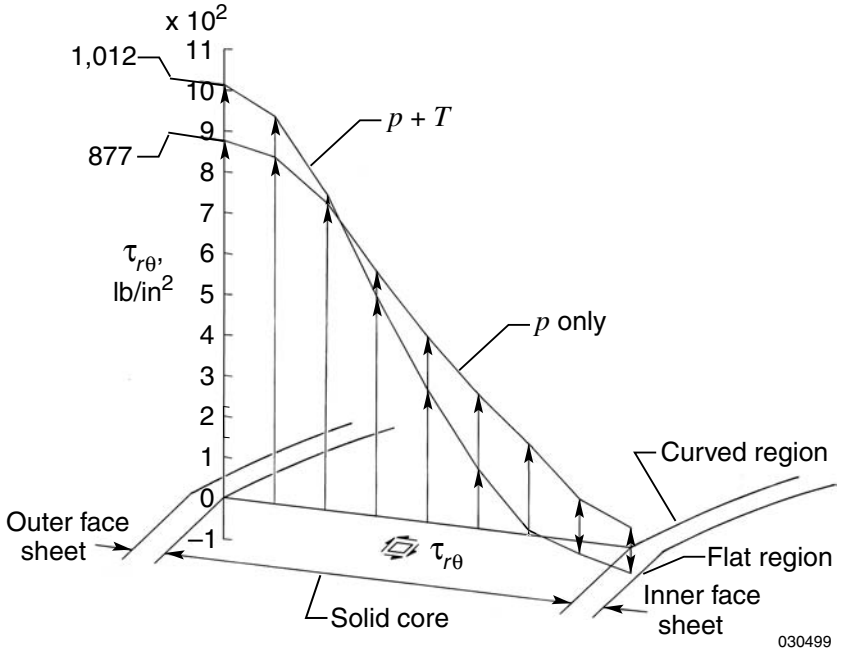

Figure 24. Radial distribution of shear stresses $\tau_{r\theta}$ at curve-flat juncture; combined internal pressure and temperature loading; p = 42 lb/in^2, T_1 = –423 °F, T_2 = 70 °F; solid corner.

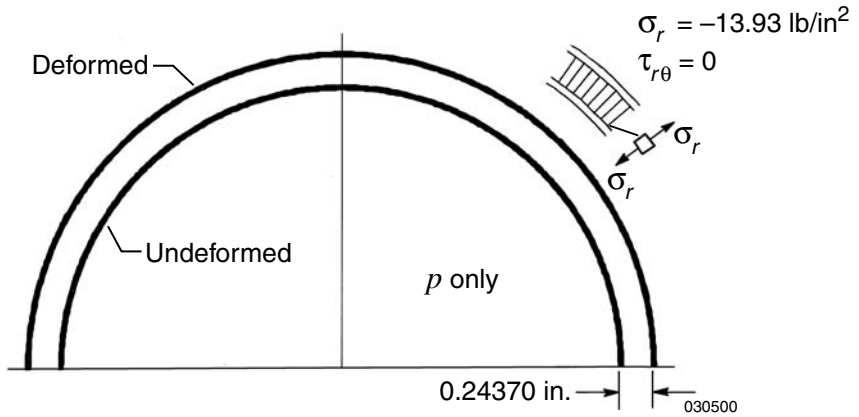

Figure 25. Deformed shape of circular cylindrical sandwich composite tank under internal pressure loading only; p = 42 lb/in^2.

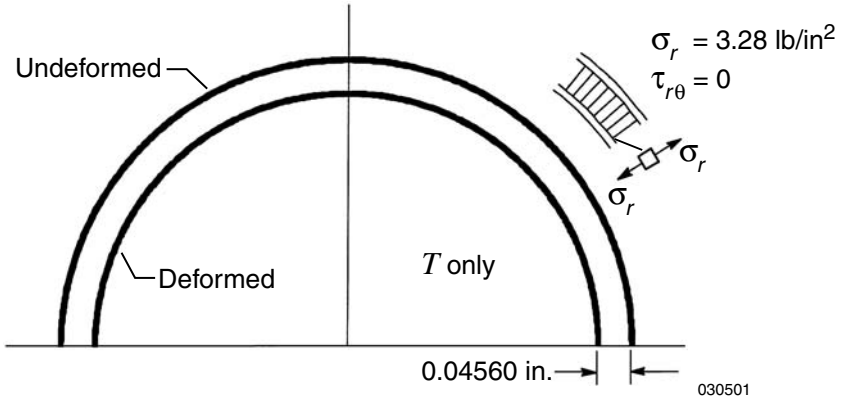

Figure 26. Deformed shape of circular cylindrical sandwich composite tank under temperature loading only; T_1 = –423 °F, T_2 = 70 °F.

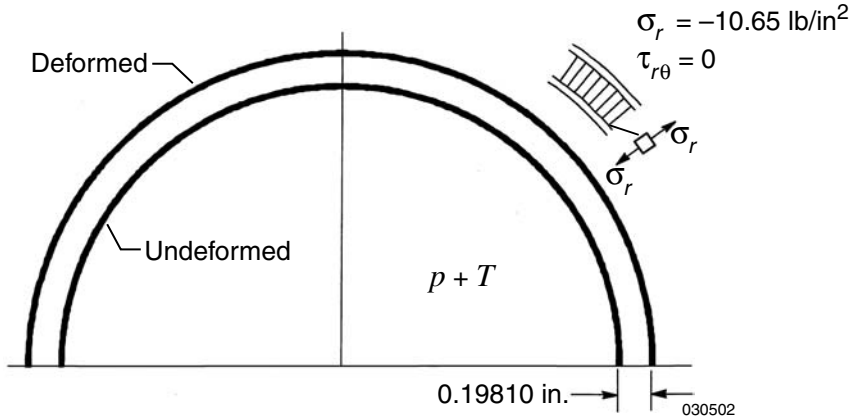

Figure 27. Deformed shape of circular cylindrical sandwich composite tank under combined internal pressure and temperature loading; p = 42 lb/in^2, T_1 = –423 °F, T_2 = 70 °F.

APPENDIX

FAILURE STRENGTHS OF SANDWICH PANELS

For background information, the delamination stress of a laminated carbon-epoxy composite using a C-shaped test coupon is approximately 5,000 lb/in^2 (ref. 8). The flat-wise tensile strengths (the pulling apart of two face sheets in the core thickness direction equals the open-mode strength) and shear strengths of typical honeycomb core sandwich panels are listed in table A-1 (ref. 9).

Table A-1. Failure strengths of typical honeycomb core sandwich panels.

Honeycomb core material	Flat-wise tensile strength, lb/in^2	Shear strength, lb/in^2
Glass-polyimide	521	3,188
Titanium	2,098	4,330

REFERENCES

1. Ko, William L., *Delamination Stresses in Semicircular Laminated Composite Bars*, NASA TM-4026, 1988.

2. Ko, William L. and Raymond H. Jackson, *Multilayer Theory for Delamination Analysis of a Composite Curved Bar Subjected to End Forces and End Moments*, NASA TM-4139, 1989.

3. O'Brien, T. K., "Characterization of Delamination Onset and Growth in a Composite Laminate," *Special Technical Testing Publication 775*, American Society for Testing and Materials, 1982, pp. 140–167.

4. O'Brien, T. K., *Interlaminar Fracture of Composites*, NASA TM-85768, 1984.

5. Tolf, G., "Stresses in a Curved Laminated Beam," *Fibre Science and Technology*, vol.19, no. 4, 1983, pp. 243–327.

6. Ko, William L. and Raymond H. Jackson, *Open-Mode Delamination Stress Concentrations in Horseshoe and Elliptic Composite Curved Bars Subjected to End Forces*, NASA TM-4164, 1990.

7. Ko, William L., *Open-Mode Debonding Analysis of Curved Sandwich Panels Subjected to Heating and Cryogenic Cooling on Opposite Faces*, NASA TP-1999-206580, 1999.

8. Hiel, Clement C., Mark Sumich, and David P. Chappell, "A Curved Beam Test Specimen for Determining the Interlaminar Tensile Strength of a Laminated Composite," *Journal of Composite Materials*, vol. 25, July 1991, pp. 854–868.

9. Payne, L., *Fabrication and Evaluation of Advanced Titanium and Composite Structural Panels*, NASA CR-166106, 1983.

10. Whetstone, W. D., *SPAR Structural Analysis System Reference Manual*, System Level 13A, vol. 1, Program Execution, NASA CR-158970-1, 1978.

11. Ko, William L., *Heat Shielding Characteristics and Thermostructural Performance of a Superalloy Honeycomb Sandwich Thermal Protection System (TPS)*, NASA/TP-2004-212024.

REPORT DOCUMENTATION PAGE

Form Approved
OMB No. 0704-0188

1. AGENCY USE ONLY (Leave blank)	2. REPORT DATE	3. REPORT TYPE AND DATES COVERED
	May 2004	Technical Publication

4. TITLE AND SUBTITLE

Debonding Stress Concentrations in a Pressurized Lobed Sandwich-Walled Generic Cryogenic Tank

5. FUNDING NUMBERS

090-50-00-SE-RR-00-000

6. AUTHOR(S)

William L. Ko

7. PERFORMING ORGANIZATION NAME(S) AND ADDRESS(ES)

NASA Dryden Flight Research Center
P.O. Box 273
Edwards, California 93523-0273

8. PERFORMING ORGANIZATION REPORT NUMBER

H-2548

9. SPONSORING/MONITORING AGENCY NAME(S) AND ADDRESS(ES)

National Aeronautics and Space Administration
Washington, DC 20546-0001

10. SPONSORING/MONITORING AGENCY REPORT NUMBER

NASA/TP-2004-212849

11. SUPPLEMENTARY NOTES

12a. DISTRIBUTION/AVAILABILITY STATEMENT

Unclassified—Unlimited
Subject Category 39

This report is available at http://www.dfrc.nasa.gov/DTRS/

12b. DISTRIBUTION CODE

13. ABSTRACT (Maximum 200 words)

A finite-element stress analysis has been conducted on a lobed composite sandwich tank subjected to internal pressure and cryogenic cooling. The lobed geometry consists of two obtuse circular walls joined together with a common flat wall. Under internal pressure and cryogenic cooling, this type of lobed tank wall will experience open-mode (a process in which the "honeycomb" is stretched in the depth direction) and shear stress concentrations at the junctures where curved wall changes into flat wall (known as a curve-flat juncture). Open-mode and shear stress concentrations occur in the honeycomb core at the curve-flat junctures and could cause debonding failure. The levels of contributions from internal pressure and temperature loading to the open-mode and shear debonding failure are compared. The lobed fuel tank with honeycomb sandwich walls has been found to be a structurally unsound geometry because of very low debonding failure strengths. The debonding failure problem could be eliminated if the honeycomb core at the curve-flat juncture is replaced with a solid core.

14. SUBJECT TERMS	15. NUMBER OF PAGES
Composite honeycomb sandwich wall, Lobed cryogenic tank, Open-mode debonding, Stress concentrations, Thermocryogenic stress analysis	34
	16. PRICE CODE

17. SECURITY CLASSIFICATION OF REPORT	18. SECURITY CLASSIFICATION OF THIS PAGE	19. SECURITY CLASSIFICATION OF ABSTRACT	20. LIMITATION OF ABSTRACT
Unclassified	Unclassified	Unclassified	Unlimited